Research Square

Preprints are preliminary reports that have not undergone peer review.
They should not be considered conclusive, used to inform clinical practice,
or referenced by the media as validated information.

Fabrication of Conductive Polyaniline Nanomaterials based on Redispersed Cellulose Nanofibrils

Ping Wang
South China University of Technology
Hefang Liu
South China University of Technology
Wenhua Gao (segaowenhua@scut.edu.cn)
South China University of Technology
Jinsong Zeng
South China University of Technology
Bin Wang
South China University of Technology
Jun Xu
South China University of Technology
Zhiwei Wang
Guangxi University

Research Article

Keywords: Cellulose nanofibrils, Redispersion, Poly(vinylpyrrolidone), Conductive nanomaterials

Posted Date: May 17th, 2022

DOI: https://doi.org/10.21203/rs.3.rs-1552244/v1

License: This work is licensed under a Creative Commons Attribution 4.0 International License.
Read Full License

Abstract

Dewatering or drying of diluted cellulose nanofibril suspensions is an effective way for reducing the costs of transportation and storage. In this study, poly(vinylpyrrolidone) (PVP) was introduced into a redispersing system of concentrated CNFs, and the obtained redispersed CNFs were used for fabricating CNF/PANI (polyaniline) nanomaterials by in situ polymerization method. The results showed that mechanical grinding with grinding gap of -20 μm was an effective way to redisperse the concentrated CNFs, especially when the PVP was added in the redispersing process. The conductivity of the redispersed CNF/PANI film reached 1.08 S/cm and the specific capacitance reached 118.3 F/g (at 0.3 A/g), when the concentrated CNFs were redispersed with 5% PVP. During the polymerization process, PVP facilitated the PANI coating on the CNFs uniformly as steric stabilizer. This study provided a basis for the application of redispersed CNFs in conductive nanomaterials area.

1. Introduction

Cellulose nanofibrils (CNFs) as a kind of nanocellulose are usually disintegrated from cellulosic fibers by mechanical process based on chemical or enzymatic pretreatment. Due to the high aspect ratio, entangled network structure, and abundant hydroxyl groups, CNFs have been attracted considerable attention in many fields, such as biomedicine, packaging, papermaking, cosmetics, food, conductive bio-nanomaterials, etc.[1–5] Generally, the prepared CNFs are stored in a form of aqueous suspension and have a water content greater than 98%.[6] The low solid content of CNF suspension leads to high transport and storge costs, which limits the end-usage application of CNFs. In order to facilitate the commercialization of CNFs, many dehydration methods are applied to dry the CNF suspension including oven drying, freeze drying, spray drying, and supercritical drying.[7] In the drying process, the agglomeration of CNFs were inevitable, and the drying strategies of adding additives[8–10] or modifications[11–13] of CNFs were proposed. For example, the replacement of water in CNF suspension with PEG[14] and protonation[15] had also been investigated to inhibit CNF agglomerations. However, dehydration of CNF suspension always leads to severe irreversible agglomeration due to the formation of hydrogen bonds between adjacent fibrils.[16–17] In order to reduce the agglomeration degree of CNF suspension, concentration process can be proposed to obtain high solid content CNF suspension instead of dehydration process.[18] How to maintain the original structure and morphology of concentrated CNFs is a challenge for CNF end-use application.[19] Therefore, the development of low-cost, efficient and non-destructive redispersing methods of concentrated CNF suspension is essential for commercialization of CNFs. Poly(vinylpyrrolidone) (PVP) is a nonionic water-soluble polymer and is usually used as a suspension dispersant.[20–21] Previous study showed CNF film had a relatively smooth surface in the presence of PVP.[22] Besides, in the process of preparation of conductive polymers, PVP has steric stabilizing effects that promotes a uniform growth of conductive polymers.[23–24]

As a conductive polymer, polyaniline (PANI) has attracted a lot of attention due to its low cost, easy synthesis, and conductivity. The redox reaction of PANI during charge/discharge process endows

conductive material with pseudo capacitance, and thus enhances the capacitance.[25] However, neat PANI has poor film-forming capability limiting its application. The web-like CNFs with abundant hydroxyl groups could be chosen as a promising template for the polymerization of aniline monomer.[26–28] In the process of polymerization, the hydrogen bonds are formed between hydroxyl groups of CNFs and amine groups of PANI, and ensures continuous conductive network. Besides, the flexible CNF/PANI conductive nanomaterial had remarkable mechanical properties, lightweight and environmental stability, showing great potential application in electronic devices.

In this work, we developed a facile process for concentrating-redispersing CNFs aiming to efficiently utilize redispersed CNFs for synthesizing conductive polymer nanomaterials. CNF suspension was concentrated by a centrifuge and redispersed by a grinding process. PVP was used as dispersant in redispersing process, and the redispersed CNFs were further submitted to synthesize CNF/PANI conductive nanomaterials. PVP had a function of alleviating the agglomeration of PANI during the polymerization, which may facilitate the construction of continuous conductive network. This study can provide technical and theoretical support for the large-scale production and application of CNF based nanocomposites.

2. Experimental

2.1 Materials

The commercial bleached softwood kraft pulp (BSKP) was obtained from a paper company (Guangdong, China) and used for the preparation of CNFs. Commercial endoglucanase (enzyme activity 7.3 IU/ml) was acquired from Paper Chemical Co., Ltd (Jiangsu, China). Aniline, ammonium persulfate [$(NH_4)_2S_2O_8$, APS], Congo red with a relative molecular weight of 696.66 and poly(vinylpyrrolidone) (PVP) with a relative molecular weight of 58000 were purchased from Macklin Biochemical Co., Ltd (Shanghai, China). Other chemicals were analytical grade.

2.2 Preparation of CNFs

The dry BSKP was immersed in water with a concentration of 3.0 wt% for overnight. Then the pulp was defibered by a lab Valley Beater (Voith Inc., Appleton, WI, USA) for 15 min. The enzymatic pretreatment was carried out based on previous report with some modifications.[29] A certain amount of pretreated pulp was immersed in 50 mM citric acid-sodium citrate buffer solution (pH 5.2) to reach a concentration of 4.0 wt% and the endoglucanase loading was 9 mg/g substrate. The slurry was continuously agitated in a water bath at 50 °C for 2 h. After enzymatic pretreatment, the slurry was placed in a water bath at 85 °C for 15 min to denature the endoglucanase. The obtained pulp was washed with distilled water until the extruded water was natural and stored at 4 °C. The pretreated pulp was diluted to a concentration of 1.0 wt% and mechanically fibrillated using a super masscolloider (MKCA 6 − 2 J, Masuko Sangyo Co., Ltd, Japan). The gap of discs was adjusted from 0 to -100 μm. Finally, CNFs were obtained by passing grinder 15 times with a gap of -100 μm at 2000 rpm.

2.3 Concentration and redispersion of CNFs

The obtained CNF (CNF_{ND}) suspension was added into a 10000-mesh polypropylene fiber bag, and then concentrated by a centrifuge (PSB300N, China) for 15 min at the centrifugal force of 10000 g. The concentrated CNFs were diluted to 0.5 wt% with distilled water, and mechanically stirred at 300 rpm for 30 min labeled as CNF_{MS}. The diluted CNFs were grinded by the supermasscolloider with the disc gap of 0, -20, -50 μm for 5 times at 800 rpm, respectively. The dispersed CNFs obtained by grinding under different gaps was named as $CNF_{R(0)}$, $CNF_{R(-2)}$ and $CNF_{R(-5)}$, respectively. In addition, prior to mechanical stirring, 5% or 10% PVP (relative to the oven dried CNFs) was added to CNF suspension to investigate its role in the dispersion of CNFs. The samples added with 5% and 10% PVP were grinded with the disc gap of -20 μm, and labeled as $CNF_{R(-2)-5PVP}$ and $CNF_{R(-2)-10PVP}$.

2.4 Preparation of CNF films

The CNF films were prepared by vacuum filtration and subsequent hot pressing. The original and redispersed CNF suspensions were filtered through a 0.45 μm hydrophilic filter membrane (CA, Shanghai, China). After filtration, wet cakes loaded with a certain weight were heated on a heating plate at 80 °C for 20 h.

2.5 Preparation of CNF/PANI conductive nanomaterials

The CNF/PANI conductive nanomaterials were prepared by in situ polymerization in the presence of APS as an oxidant and hydrochloric acid (HCl) as a dopant. Aniline monomer (0.25 g) was added into 5 ml 2 M HCl solution, and then dissolved in CNF suspension. The mass ratio of CNF/PANI was 1:1. The solution was stirred for 30 min at the temperature of 5 °C. The polymerization was initiated by adding 0.78 g APS (dissolved in 5 ml 2 M HCl). The molar ratio of APS/aniline was 1.25:1, and the final CNF concentration was adjusted to 0.3 wt%. After 90 min polymerization reaction, the dark green solution was filtered and washed with deionized water. Composite film was prepared by hot pressing.

2.6 Characterization

Atomic force microscopy (AFM, Bruker, Germany) was used for analyzing the morphology of CNFs. The diameters of CNFs were obtained by measuring its width. 100–110 nanofibrils were measured by nonomeasure software 1.2. Transmittance of CNF suspensions (0.1 wt%) and films (60 g/m^2) were performed on a UV-Vis spectrophotometer (UV-1900, China) in the wavenumber between 400 and 800 nm. Films were cut into 35 · 8 mm and were equilibrated at 23 ± 2 °C and 50 ± 2% RH for more than 48 h, and then tensile strength were performed with a span length of 15 mm at a stretched speed of 5 mm/min on a Tensile Compressive Universal Testing Machine (INSTRON 3342, USA). Fourier transform infrared (FTIR) spectra was acquired by a spectrophotometer (FT-IR 4700, Japan) in the wavenumber range 4000 to 500 cm^{-1} with a resolution of 4 cm^{-1} at 25 °C. The surface morphologies of CNF films and CNF/PANI nanomaterials were characterized by Field-emission scanning electron microscopy (FE-SEM, Merlin, Zeiss, Germany). Before FE-SEM test, a thin gold layer was sputtered on the samples and then operated at an accelerating voltage of 10 KV.

The specific surface area (SSA) was determined by the Congo red adsorption method, as reported by Wang.[30] A certain amount of CNF suspension was mixed with Congo red solution and incubated at 60 °C for 24 h in an orbital shaker. To remove the unabsorbed Congo red, the suspension was centrifuged at 10000 rpm for 15 min. The concentration of the supernatant was calculated from the standard curve. The absorbance of standard solution and supernatant were determined at 495 nm using an UV-Vis spectrophotometer (UV-2600, China). SSA (m^2/g) was calculated according to the following Eq. (1),

$$SSA = \frac{N_A m_1 A_d}{M_\omega} \quad (1)$$

where N_A is Avogadro's constant ($6.022´10^{23}$ mol^{-1}), m_1 is the saturated absorption value (g/Kg), A_d is the surface area of one Congo red molecule (1.73 nm^2), M_w is the molecular weight of Congo red, 696.66 g/mol.

The zeta potential of CNFs was measured by a Fiber Potential Analyzer (FPA, Germany). Each sample was measured at a concentration of 0.5 wt%.

The water retention value (WRV) was measured by a centrifugal method.[31] A certain amount of CNF suspension was wrapped in a 5000-mesh nylon bag and placed in a centrifuged tube with a metal mesh in the middle to allow water to accumulate at the bottom of the tube. All samples were concentrated with the centrifugal force of 3000 g for 15 min by a centrifuge (Cence, H2050R, China). The centrifuged CNF gel was weighed before and after drying in an oven at 105 °C, respectively. The WRV was calculated from the following Eq. (2),

$$WRV = \frac{m_{wet} - m_{dried}}{m_{dried}} \times 100\% \quad (2)$$

where m_{wet} and m_{dried} are the weights of centrifuged CNF samples before and after oven drying, respectively.

The X-ray diffraction (XRD) measurement was performed on an X-ray diffractometer (X'pert powder, PANalytical, Netherlands), which was operated at 40 KV and 40 mA. The diffracted intensity of Cu Ka radiation was measured in a 2q range between 5° and 40° at a scanning rate of 12°/min. The crystallinity index (CrI) was calculated by using the following Eq. (3) :[32]

$$CrI = \frac{I_{002} - I_{am}}{I_{002}} \times 100\% \quad (3)$$

where I_{200} is the maximum intensity of 002 plane at 2θ around 22.5°, and I_{am} is the minimum intensity at 2θ close to 18.5° which represents the amorphous regions. The crystallite sizes (D_{hkl}) of the crystal in 002 lattice planes were calculated according to Scherrer Eq. (4):[33–34]

$$\mathrm{Dhkl} = \frac{0.9}{\cos} \qquad (4)$$

where λ is the radiation wavelength (0.15418 nm), β is the width of half-maximum intensity in radians and θ is the diffraction angle.

2.7 Electrochemical Tests

The conductivity of composite film was measured by a four-point probe (KDY-1, China). Cyclic voltammetry (CV) and galvanostatic charge/discharge (GCD) tests were carried on an electrochemical workstation (CHI660E, China). The composite film, Pt foil and Ag/AgCl electrode were used as working electrode, counter electrode and reference electrode, respectively. 2 M H_2SO_4 was used as the electrolyte. CV tests were conducted in the potential window of -0.3 to 0.7 V at different scan rates of 10, 20, 30, 50, 100, 200 mV/s. The specific capacitance (C_{Scv}, F/g) of each sample can be calculated from the CV curve and the equation is as follows:

$$\mathrm{CScv} = \frac{\int IdV}{mv\overline{V}} \qquad (5)$$

where $\int IdV$ is the integrated area of the CV curve, v is the scan rate (mV/s), m is the mass of active material (g), and ΔV is the potential window (V).

The galvanostatic charge/discharge tests were performed in the potential range of from − 0.3 V to 0.7 V at different current density. The specific capacitance (C_{Sgcd}, F/g) calculated from GCD curve is as follows:

$$\mathrm{CSgcd} = \frac{I\mathrm{t}}{m\overline{\mathrm{V}}} \qquad (5)$$

where I is the constant current from discharge (A), Δt is the discharge time (s), m is the mass of the active material (g), and ΔV is the voltage of discharge excluding voltage drop (V).

3. Results And Discussion

3.1 Effect of redispersion on the properties of CNFs

Specific surface area (SSA) was an effective method to characterize the redispersion of CNFs.[8–9] In this study, SSA of CNFs was obtained by Congo red adsorption method. As seen in Table 1, CNF_{MS} showed the lowest SSA of 87.39 m^2/g, which indicated that mechanical stirring could not effectively redisperse the agglomerations of CNFs. The shrinkage of the exposed CNFs surface caused by hydrogen bonding is the main reason for the decrease of SSA.[10] The SSA of CNFs was affected by grinding parameters. The SSA of redispersed CNFs tended to increase with the grinding gap decrease. It was noteworthy that the SSA of $CNF_{R(-5)}$ (106.93 m^2/g) was higher than that of CNF_{ND} (104.66 m^2/g). The grinding fibrillation method was effective in improving the SSA of redispersed CNFs.

In the process of CNF concentration, with the removal of water, the fibers gradually get together and form hydrogen bonds between fibrils. This leaded to fibril aggregation and influenced the swelling ability of CNFs. WRV was used to evaluated the effect of grinding treatment on the redispersion of concentrated CNFs. The WRV results of redispersed CNFs were shown in Table 1. The WRV of CNF_{MS} was 531.01%, which was 68.97% lower than that of CNF_{ND} (599.98%), which indicated that the concentrated CNFs maybe not totally redispersed by the treatment of mechanical stirring. However, WRV of redispersed CNFs significantly increased from 555.79–647.00% with the reduction of grinding gap. Grinding treatment was an effective way to redisperse the concentrated CNFs, and realized the concentrated CNFs had micro/nano scale and relatively uniform distribution again.[35] Additionally, grinding treatment leaded to extended fibrillation of CNFs, resulting in SSA increasing. This was consistent with previous research that WRV was depended on the fibrillation of fibers to some extent.[31]

Zeta potential was used to characterize the surface charge of fibers. CNFs exhibited negative zeta potential, which was attributed the hydroxyl groups on fiber surface. Zeta potential of initial and redispersed CNFs were listed in Table 1. The zeta potential of CNF_{ND} was − 34.3 mV. CNF_{MS} had a zeta potential of -26.4 mV, which indicated that the agglomeration had a negative effect on the absolute value of zeta potential. When non-ionic PVP added, the absolute value of zeta potential decreased significantly, indicating that PVP adsorbing onto the CNFs surface. Fibers with the same electric charge repelled each other by the electrostatic repulsion, and thus affected the dispersion stability of CNF suspension.[36] As seen in Fig. 1a, the CNF stability was enhanced as the redispersed condition became intense. Most of hydrogen bonds formed during concentration may be broken in the grinding process, leading the increase of the absolute value of zeta potential (Table 1). When PVP was added in the redispersion process, the redispersed CNFs showed high stability especially with the dosage of PVP increasing (Fig. 1a). Although PVP reduces the zeta potential, it acted as a dispersant and provided steric barriers between fibrils. Based on the results, the possible mechanism of PVP action on the stability of CNF suspension was obtained and shown in Fig. 1b.

Table 1
The properties of initial and redispersed CNFs

Samples	Zeta potential (mV)	SSA (m^2/g)	WRV (%)	CrI (%)	D_{hkl} (nm)	Tensile strength (Mpa)
CNF_{ND}	-34.3 ± 0.3	104.66 ± 0.27	599.98 ± 2.19	68.34	3.02	105.96 ± 1.13
CNF_{MS}	-26.4 ± 0.2	87.39 ± 0.78	531.01 ± 8.78	71.75	3.20	42.5 ± 3.74
$CNF_{R(0)}$	-32.4 ± 0.5	94.74 ± 0.40	555.79 ± 12.63	71.56	3.16	84.03 ± 1.23
$CNF_{R(-2)}$	-35.6 ± 0.1	97.69 ± 0.59	556.87 ± 2.32	71.21	3.14	87.82 ± 8.71
$CNF_{R(-5)}$	-36.8 ± 0.3	106.93 ± 0.43	647.00 ± 2.33	69.74	3.03	112.89 ± 2.68
$CNF_{R(-2)-5PVP}$	-32.7 ± 0.2			70.84	3.13	103.37 ± 6.02
$CNF_{R(-2)-10PVP}$	-24.5 ± 0.2			70.83	3.12	109.22 ± 3.04

The transmittance of CNF suspension was a typical representation for the dispersion of CNF particles.[37] Fig. 2 showed the transmittance of CNF suspensions. The results showed that the redispersing property of CNF suspension was consistent with the transmission performance. The CNFs with small and uniform size was much stable, which reduced the light scattering and benefited for improving the transmittance. This result is consistent with the previous reports.[38]

AFM images were used to characterize the morphologies of initial and redispersed CNFs, and the diameter distribution of CNFs was determined. As seen in Fig. 3a, CNF_{ND} with a mean diameter (MD) of 42.57 nm exhibited good uniformity. After concentration and mechanical stirring, CNF_{MS} showed aggregation performance (Fig. 3b) due to the forming of hydrogen bonds between fibrils. The fiber bundles enabled CNF_{MS} to have a high MD up to 97.28 nm. It indicated that the agglomerations between fibers were difficult to redisperse in the stirring process. The MD of $CNF_{R(0)}$, $CNF_{R(-2)}$ and $CNF_{R(-5)}$ were 66.60, 50.69 and 42.27 nm, respectively. Figure 3c, d and **e** revealed that the agglomerations significantly decreased with the decrease of grinding gap. The grinding fibrillation process was benefit for forming uniform diameter distribution of redispersed CNFs. This also supported the results of WRV (Table 1). $CNF_{R(-2)}$, $CNF_{R(-2)-5PVP}$ and $CNF_{R(-2)-10PVP}$ had similar diameter distribution. High dosage of PVP resulted in the self-agglomeration, which was denoted by green arrows in AFM image of $CNF_{R(-2)-10PVP}$ sample (Fig. 3g).

3.2 Chemical and crystalline structures of redispersed CNFs

The chemical bonds of initial and redispersed CNFs were analyzed by FTIR. FTIR spectra of PVP, initial and redispersed CNFs were exhibited in Fig. 4a. The characteristic absorption peaks at 1665 and 1288

cm^{-1} were assigned to the stretching of C = O and C-N of PVP, respectively. A large absorption peak at 3400 cm^{-1} indicated that PVP contained absorbed water.[39] The peaks at 3329 and 1900 cm^{-1} were attributed to O-H vibration and C-H stretching of CNFs, respectively. Other typical cellulose peaks were observed at 2900 cm^{-1} (C-H stretching), 1427 cm^{-1} (-CH_2 and -OCH in-plain deformation), 1369 cm^{-1} (C-H deformation vibration) and 1051 cm^{-1} (C-O-C pyranose ring skeletal vibration). The spectrum of $CNF_{R(-2)}$ was similar to that of CNF_{ND}, indicating that the chemical structure did not change in the redispersion process. The O-H vibration of $CNF_{R(-2)-5PVP}$ and $CNF_{R(-2)-10PVP}$ was shifted to 3333 cm^{-1} and 3336 cm^{-1}, respectively, which indicated that the new interaction between amide groups of PVP and hydroxyl groups of CNFs weakened the interfibrillar hydrogen bonds. In addition, the band at 1105 cm^{-1} are related to the C-O-C glycosidic ether linkages.[40] When PVP was added, the C-O-C group of $CNF_{R(-2)-10PVP}$ showed a 1 cm^{-1} high-wavenumber-shift to 1106 cm^{-1}, which may be attributed to the weakening of hydrogen bond between C-O-C groups and hydroxyl groups.[41]

The crystalline structure of initial and redispersed CNF films was characterized by XRD. The XRD patterns of CNFs treated with different redispersing process are shown in Fig. 4b. The diffraction peaks of all samples at 2θ = 15.1°, 16.5°, 22.5° are corresponding to (1̄10), (110), (200) lattice plane, respectively, suggesting that initial and redispersed CNFs are typical cellulose I crystalline form. The concentration-redispersion process resulted in changes in crystallinity (CrI) and crystallite size (D_{hkl}). All the samples had CrI range from 68.34 to 71.75% and D_{hkl} range from 3.02 to 3.20 nm (Table 1**)**. The CNF_{MS} had the highest CrI and D_{hkl}. When the CNF suspension was redispersed by grinding, the CrI and D_{hkl} of CNFs decreased significantly. The results proved that the intermolecular and intramolecular hydrogen bonds were formed in the process of concentration, and some of the hydrogen bonds were broken during the redispersion process. The CrI of $CNF_{R(-2)-5PVP}$ and $CNF_{R(-2)-10PVP}$ were lower than that of $CNF_{R(-2)}$, which was ascribed to the amorphous nature of PVP.

3.3 Properties of CNF films

The transmittance of CNF films (Fig. 5a) is also determined by the diameter distribution of CNFs. Fibril agglomerations were observed in CNF_{MS}, $CNF_{R(0)}$ and $CNF_{R(-2)}$ films (Fig. 5e, f, g), leading to the transmittance of films decreasing. When 5% PVP was added to redisperse CNFs, the surface of $CNF_{R(-2)-5PVP}$ film (Fig. 5i, j) became smoother and more uniform than that of $CNF_{R(-2)}$ film and was similar to that of CNF_{ND} film (Fig. 5c, d). Therefore, $CNF_{R(-2)-5PVP}$ film had higher transmittance than $CNF_{R(-2)}$ film. The addition of PVP can improve the redispersed CNF film transmittance.

The stress-strain curves of films prepared from initial and redispersed CNF suspensions were shown in Fig. 5b. The tensile strength was listed in Table 1. The films prepared by CNFs with high dispersibility degree showed high tensile strength. $CNF_{R(-2)}$ film had a tensile strength of 87.82 MPa. With the additions of 5% and 10% PVP, the tensile strength was increased to 103.37 and 109.22 MPa, respectively. It was expected that the dispersing effect of PVP further increased the tensile strength of redispersed CNF films.[22]

3.4 The electrochemical performance of redispersed-CNF/PANI nanomaterials

CNF/PANI flexible nanomaterials (Fig. 6b) were prepared by in situ polymerization. CNFs are supposed to be a promising template for loading PANI due to high surface area and luxuriant hydroxyl groups.[42–43] As discussed above, the grinding gap of -20 μm was chosen to be an appropriate process to redisperse concentrated CNFs. $CNF_{R(-2)}$, $CNF_{R(-2)-5PVP}$ and $CNF_{R(-2)-10PVP}$ were used to prepare PANI nanomaterials. And the CNF_{ND} was regarded as reference substance to study the effect of redispersion on the electrochemical performances of PANI nanomaterials. As seen in Fig. 6a, the conductivity of $CNF_{R(-2)}$/PANI was 0.64 S/cm, which was lower than CNF_{ND}/PANI (0.83 S/cm). The reduction of specific surface area due to irreversible aggregation was responsible for the reduction of conductivity. In addition, compared with CNF_{ND}/PANI (Fig. 6c), $CNF_{R(-2)}$/PANI (Fig. 6d) had an irregular and heterogeneous surface morphology due to fibril agglomerations, which indicated that non-continuous conducting network reduced the conductivity. Redispersed CNFs containing PVP were used to fabricate conductive nanomaterials. A noticeable homogeneous surface was observed in Fig. 6e for $CNF_{R(-2)-5PVP}$/PANI. With increasing the addition of PVP to 10%, PANI was uniformly coated on the surface of CNFs. The $CNF_{R(-2)-10PVP}$/PANI had a low conductivity of 0.75 S/cm, which may attribute to the excessive non-conductive PVP block the absorption of PANI. In the process of redispersion and polymerization, PVP has two functions: firstly, it was used as dispersant to stable the CNF suspension for further polymerization; secondly, it acted as steric stabilizer to facilitate the uniform polymerization of PANI on the CNF surface (Fig. 6g).[23] As seen in Fig. 6h, the hydrogen bonds between CNF, PANI and PVP might severe as traction force to form an integrated 3D network, which contribute to the formation of continues conducting routes. The conductivity of redispersed-$CNF_{R(-2)-5PVP}$/PANI was as high as 1.08 S/cm, which is an order of magnitude higher than previous reports at the same PANI content.[27, 44]

CV measurement was used to evaluate the electrochemical performance of CNF/PANI nanomaterials in a three-electrode system. Figure 7a showed the CV curves of CNF_{ND}/PANI electrode in a potential range of -0.3–0.7 V at different scan rates. There were obvious redox peaks on the CV curves, suggesting ideal pseudo capacitances from PANI.[45–46] The comparisons of CNF_{ND}/PANI, $CNF_{R(-2)}$/PANI, $CNF_{R(-2)-5PVP}$/PANI and $CNF_{R(-2)-10PVP}$/PANI nanomaterials were shown in CV curves at a scan rate of 30 mV/s (Fig. 7b**)**. The C_{Scv} of CNF_{ND}/PANI at 30 mV/s was 14.3 F/g. After dewatering-redispersing process, the C_{Scv} of $CNF_{R(-2)}$/PANI decreased to 4.2 F/g at 30 mV/s due to the agglomeration. $CNF_{R(-2)-5PVP}$/PANI composite electrode possessed the highest C_{Scv} of 17.6 F/g at 30 mV/s. The excellent capacitive performance of $CNF_{R(-2)-5PVP}$/PANI was ascribed to the uniform coating of PANI, which promoted the electrolyte contact and ion diffusion.[47] The changes of C_{Scv} at different scan rates were shown in Fig. 7c. When the addition of PVP increased to 10%, the C_{Scv} of $CNF_{R(-2)-10PVP}$/PANI (14.6 F/g) decreased. High PVP content leaded to discontinues conductive network, and impeded the charge transmission.

To further investigate the effect of redispersion on the capacitance performance of composite electrode, GCD measurement was carried out at various current density. As seen in Fig. 7d, the charge/discharge curves were asymmetric triangles, indicating the presence of pseudo capacitance caused by redox reaction of PANI.[48–49] As the charge/discharge procedure, the time required gradually decreased with the increase of current density, which was similar to the previous report.[50] The C_{Scd} of the CNF_{ND}/PANI, $CNF_{R(-2)}$/PANI, $CNF_{R(-2)-5PVP}$/PANI and $CNF_{R(-2)-10PVP}$/PANI electrodes were 83.6, 60.0, 118.8 and 97.8 F/g at the current density of 0.3 A/g, respectively. This agrees with the results of C_{Scv} obtained from CV measurements. The capacitance of redispersed-$CNF_{R(-2)-5PVP}$/PANI was higher than the previous reported CNF/PANI/reduced graphene oxide composite (79.71 F/g).[51] As the scan rate and current density increase, the C_{Scv} and C_{Scd} (Fig. 7c, f) decreased sharply, which was attributed to the hot-pressing, thereby reducing the porosity of nanomaterials. This further slowed down ion transport and reduced charge storage capacity at high scan rate or current density.[52]

4. Conclusion

A mild redispersion method of concentrated CNFs and its application in PANI conductive nanomaterial have been developed in this study. The redispersing process is very essential for the specific surface area, water retention value, zeta potential value, and fibril diameter. The properties of CNFs redispersed by mild grinding process (-20 μm) are almost the same with never-concentrated CNFs. PVP plays an important role in suspension stability and mechanical strength. The effect of redispersion on the electrochemical properties of CNF/PANI conductive nanomaterial was investigated. The concentration-redispersion process of CNFs had a negative effect on the electrochemical properties of conductive nanomaterials. Importantly, CNFs redispersed by adding 5% PVP resulted in significant increase in conductivity and capacitance of nanomaterials, which ascribed to the steric stabilization effect of PVP. In summary, the effective redispersed-CNFs for the synthesis of PANI nanomaterial should significantly facilitate the scalable fabrication and application of CNFs based conductive nanomaterials with high performance.

Declarations

Notes

The authors declare no competing financial interest.

ACKONWLEDGEMENT

The work was supported by the National Natural Science Foundation of China (31971603), Guangzhou Science and Technology Program (General Scientific Research Project (202102021212), Foundation of Guangxi Key Laboratory of Clean Pulp and Papermaking and Pollution Control, College of Light Industry and Food Engineering, Guangxi University, (No. 2019KF06).

References

1. Saska S, Teixeira L, de Castro Raucci L, Scarel-Caminaga R, Franchi L, Dos Santos R, Santagneli S, Capela M, de Oliveira P, Takahashi C, Gaspar A, Messaddeq Y, Ribeiro S, Marchetto R Nanocellulose-collagen-apatite composite associated with osteogenic growth peptide for bone regeneration.Int. J Biol. Macromol**2017**, *103*,467–476
2. Yu H, Zhang H, Song M, Zhou Y, Yao J, Ni Q From Cellulose Nanospheres, Nanorods to Nanofibers: Various Aspect Ratio Induced Nucleation/Reinforcing Effects on Polylactic Acid for Robust-Barrier Food Packaging.ACS Appl. Mater. Interfaces**2017**, *9* (50),43920–43938
3. Lourenço A, Godinho D, Gamelas J, Sarmento P, Ferreira P (2019) Carboxymethylated cellulose nanofibrils in papermaking: influence on filler retention and paper properties. Cellulose 26(5):3489–3502
4. Perrin L, Gillet G, Gressin L, Desobry S (2020) Interest of Pickering Emulsions for Sustainable Micro/Nanocellulose in Food and Cosmetic Applications. Polym (Basel) 12(10):1–14
5. Hassan G, Forsman N, Wan X, Keurulainen L, Bimbo L, Johansson L-S, Sipari N, Yli-Kauhaluoma J, Zimmermann R, Stehl S, Werner C, Saris P, Österberg M, Moreira V (2019) Dehydroabietylamine-Based Cellulose Nanofibril Films: A New Class of Sustainable Biomaterials for Highly Efficient, Broad-Spectrum Antimicrobial Effects. ACS Sustainable Chem Eng 7(5):5002–5009
6. Isogai A (2021) Emerging Nanocellulose Technologies: Recent Developments. Adv Mater 33(28):2000630
7. Peng Y, Gardner D, Han Y Drying cellulose nanofibrils: in search of a suitable method.Cellulose 2011, *19* (1),91–102
8. Velasquez-Cock J, Gomez HB, Posada P, Serpa GA, Gomez HC, Castro C, Ganan P, Zuluaga R (2018) Poly (vinyl alcohol) as a capping agent in oven dried cellulose nanofibrils. Carbohydr Polym 179:118–125
9. Velásquez-Cock J, Gañán P, Gómez H, Posada C, Castro P, Dufresne C, Zuluaga A (2018) Improved redispersibility of cellulose nanofibrils in water using maltodextrin as a green, easily removable and non-toxic additive. Food Hydrocoll 79:30–39
10. Kwak H, You J, Lee M, Jin H (2019) Prevention of cellulose nanofibril agglomeration during dehydration and enhancement of redispersibility by hydrophilic gelatin. Cellulose 26(7):4357–4369
11. Yan Y, Amer H, Rosenau T, Zollfrank C, Dörrstein J, Jobst C, Zimmermann T, Keckes J, Veigel S, Gindl-Altmutter W, Li J (2016) Dry, hydrophobic microfibrillated cellulose powder obtained in a simple procedure using alkyl ketene dimer. Cellulose 23(2):1189–1197
12. Wang L, Sanders J, Gardner D, Han Y (2016) In-situ modification of cellulose nanofibrils by organosilanes during spray drying. Ind Crops Prod 93:129–135
13. Eyholzer C, Bordeanu N, Lopez-Suevos F, Rentsch D, Zimmermann T, Oksman K Preparation and characterization of water-redispersible nanofibrillated cellulose in powder form.Cellulose 2009, *17* (1),19–30
14. Santmarti A, Tammelin T, Lee K (2020) Prevention of interfibril hornification by replacing water in nanocellulose gel with low molecular weight liquid poly(ethylene glycol). Carbohydr Polym

250:116870

15. Jiang F, Hsieh Y (2016) Self-assembling of TEMPO Oxidized Cellulose Nanofibrils As Affected by Protonation of Surface Carboxyls and Drying Methods. ACS Sustainable Chem Eng 4(3):1041–1049
16. Peng Y, Gardner D, Han Y, Kiziltas A, Cai Z, Tshabalala M (2013) Influence of drying method on the material properties of nanocellulose I: thermostability and crystallinity. Cellulose 20(5):2379–2392
17. Quiévy N, Jacquet N, Sclavons M, Deroanne C, Paquot M, Devaux J (2010) Influence of homogenization and drying on the thermal stability of microfibrillated cellulose. Polym Degrad Stab 95(3):306–314
18. Ding Q, Zeng J, Wang B, Tang D, Chen K, Gao W (2019) Effect of nanocellulose fiber hornification on water fraction characteristics and hydroxyl accessibility during dehydration. Carbohydr Polym 207:44–51
19. Sinquefield S, Ciesielski P, Li K, Gardner D, Ozcan S (2020) Nanocellulose Dewatering and Drying: Current State and Future Perspectives. ACS Sustainable Chem Eng 8(26):9601–9615
20. Marani D, Sudireddy B, Nielsen L, Ndoni S, Kiebach R Poly(vinylpyrrolidone) as dispersing agent for cerium-gadolinium oxide (CGO) suspensions.J Mat. S**2015**, *51* (2),1098–1106
21. Guo J, Guo Z, Wang X, Li Y, Lv Q (2015) Experimental Investigation on Thermophysical Performance of BN/EG Nanofluids Influenced by Dispersant. Appl Mech Mater 757:7–12
22. Li G, Yu D, Song Z, Wang H, Liu W (2020) Reducing formation time while improving transparency and strength of cellulose nanostructured paper with polyvinylpyrrolidone and Laponite. Carbohydr Polym 230:115580
23. Wu X, Tang J, Duan Y, Yu A, Berry R, Tam K Conductive cellulose nanocrystals with high cycling stability for supercapacitor applications.J. Mater. Chem. A**2014**, *2* (45),19268–19274
24. Ewulonu C, Chukwuneke J, Nwuzor I, Achebe C (2020) Fabrication of cellulose nanofiber/polypyrrole/polyvinylpyrrolidone aerogels with box-Behnken design for optimal electrical conductivity. Carbohydr Polym 235:116028
25. Itoi H, Maki S, Ninomiya T, Hasegawa H, Matsufusa H, Hayashi S, Iwata H, Ohzawa Y (2018) Electrochemical polymerization of pyrene and aniline exclusively inside the pores of activated carbon for high-performance asymmetric electrochemical capacitors. Nanoscale 10(20):9760–9772
26. Yu H, Chen P, Chen W, Liu Y (2014) Effect of cellulose nanofibers on induced polymerization of aniline and formation of nanostructured conducting composite. Cellulose 21(3):1757–1767
27. Gopakumar D, Pai A, Pottathara Y, Pasquini D, Carlos de Morais L, Luke M, Kalarikkal N, Grohens Y, Thomas S (2018) Cellulose Nanofiber-Based Polyaniline Flexible Papers as Sustainable Microwave Absorbers in the X-Band. ACS Appl Mater Interfaces 10(23):20032–20043
28. Wang D, Yu H, Qi D, Ramasamy M, Yao J, Tang F, Tam K, Ni Q (2019) Supramolecular Self-Assembly of 3D Conductive Cellulose Nanofiber Aerogels for Flexible Supercapacitors and Ultrasensitive Sensors. ACS Appl Mater Interfaces 11(27):24435–24446

29. Huang L, He L, Gao W, Zeng J, Wang B, Xu J, Chen K (2020) Distribution analysis of cellulose nanofibrils in paper handsheets: Dye-labeled Method. Carbohydr Polym 239:116226
30. Wang S, Gao W, Chen K, Xiang Z, Zeng J, Wang B, Xu J (2018) Deconstruction of cellulosic fibers to fibrils based on enzymatic pretreatment. Bioresour Technol 267:426–430
31. Gu F, Wang W, Cai Z, Xue F, Jin Y, Zhu J Water retention value for characterizing fibrillation degree of cellulosic fibers at micro and nanometer scales.Cellulose 2018, *25* (5),2861–2871
32. Segal L, Creely J, Martln A, Conrad C (1959) An empirical method for estimating the degree of crystallinity of native cellulose using the x-ray diffractometer. Text Res J 29:786–794
33. Yu H, Qin Z, Liu L, Yang X, Zhou Y, Yao J (2013) Comparison of the reinforcing effects for cellulose nanocrystals obtained by sulfuric and hydrochloric acid hydrolysis on the mechanical and thermal properties of bacterial polyester. Compos Sci Technol 87:22–28
34. Ten E, Jiang L, Wolcott M (2012) Crystallization kinetics of poly(3-hydroxybutyrate-co-3-hydroxyvalerate)/cellulose nanowhiskers composites. Carbohydr Polym 90(1):541–550
35. Cheng Q, Wang J, McNeel J, Jacobson P (2010) Water retention value measurements of cellulosic materials using a centrifuge technique. BioResources 5(3):1945–1954
36. Yang X, Han F, Xu C, Jiang S, Huang L, Liu L, Xia Z (2017) Effects of preparation methods on the morphology and properties of nanocellulose (NC) extracted from corn husk. Ind Crops Prod 109:241–247
37. Han J, Zhou C, Wu Y, Liu F, Wu Q (2013) Self-assembling behavior of cellulose nanoparticles during freeze-drying: effect of suspension concentration, particle size, crystal structure, and surface charge. Biomacromolecules 14(5):1529–1540
38. Zhu H, Parvinian S, Preston C, Vaaland O, Ruan Z, Hu L (2013) Transparent nanopaper with tailored optical properties. Nanoscale 5(9):3787–3792
39. Voronova M, Rubleva N, Kochkina N, Afineevskii A, Zakharov A, Surov O (2018) Preparation and Characterization of Polyvinylpyrrolidone/Cellulose Nanocrystals Composites. Nanomaterials (Basel) 8(12):1–21
40. Deepa B, Abraham E, Cordeiro N, Mozetic M, Mathew A, Oksman K, Faria M, Thomas S, Pothan L (2015) Utilization of various lignocellulosic biomass for the production of nanocellulose: a comparative study. Cellulose 22(2):1075–1090
41. Gao Y, Jin Z (2018) Iridescent Chiral Nematic Cellulose Nanocrystal/Polyvinylpyrrolidone Nanocomposite Films for Distinguishing Similar Organic Solvents. ACS Sustainable Chem Eng 6(5):6192–6202
42. Zhang K, Gu X, Dai Q, Yuan B, Yan Y, Guo M (2019) Flexible polyaniline-coated poplar fiber composite membranes with effective electromagnetic shielding performance. Vacuum 170:108990
43. Liu Z, Chen J, Zhan Y, Liu B, Xiong C, Yang Q, Hu G-H (2019) Fe3 + Cross-Linked Polyaniline/Cellulose Nanofibril Hydrogels for High-Performance Flexible Solid-State Supercapacitors. ACS Sustainable Chem Eng 7(21):17653–17660

44. Luong N, Korhonen J, Soininen A, Ruokolainen J, Johansson L-S, Seppälä J (2013) Processable polyaniline suspensions through in situ polymerization onto nanocellulose. Eur Polym J 49(2):335–344
45. Ruan C, Li P, Xu J, Xie Y (2020) Electrochemical performance of hybrid membrane of polyaniline layer/full carbon layer coating on nickel foam. Prog Org Coat 139:105455
46. Han J, Ding Q, Mei C, Wu Q, Yue Y, Xu X (2019) An intrinsically self-healing and biocompatible electroconductive hydrogel based on nanostructured nanocellulose-polyaniline complexes embedded in a viscoelastic polymer network towards flexible conductors and electrodes. Electrochim Acta 318:660–672
47. Ding Q, Xu X, Yue Y, Mei C, Huang C, Jiang S, Wu Q, Han J (2018) Nanocellulose-Mediated Electroconductive Self-Healing Hydrogels with High Strength, Plasticity, Viscoelasticity, Stretchability, and Biocompatibility toward Multifunctional Applications. ACS Appl Mater Interfaces 10(33):27987–28002
48. Liu D, Wang X, Deng J, Zhou C, Guo J, Liu P (2015) Crosslinked Carbon Nanotubes/Polyaniline Composites as a Pseudocapacitive Material with High Cycling Stability. Nanomaterials (Basel) 5(2):1034–1047
49. Chen W, Rakhi R, Alshareef H Morphology-Dependent Enhancement of the Pseudocapacitance of Template-Guided Tunable Polyaniline Nanostructures.J. Phys. Chem. C**2013**, *117* (29),15009–15019
50. Wang L, Li X, Xu H, Wang G (2019) Construction of polyaniline/lignin composite with interpenetrating fibrous networks and its improved electrochemical capacitance performances. Synth Met 249:40–46
51. Hsu H, Khosrozadeh A, Li B, Luo G, Xing M, Zhong W, An Eco-Friendly (2019) Nanocellulose/RGO/in Situ Formed Polyaniline for Flexible and Free-Standing Supercapacitors. ACS Sustainable Chem Eng 7(5):4766–4776
52. Lay M, Mendez JA, Delgado-Aguilar M, Bun KN, Vilaseca F (2016) Strong and electrically conductive nanopaper from cellulose nanofibers and polypyrrole. Carbohydr Polym 152:361–369

Figures

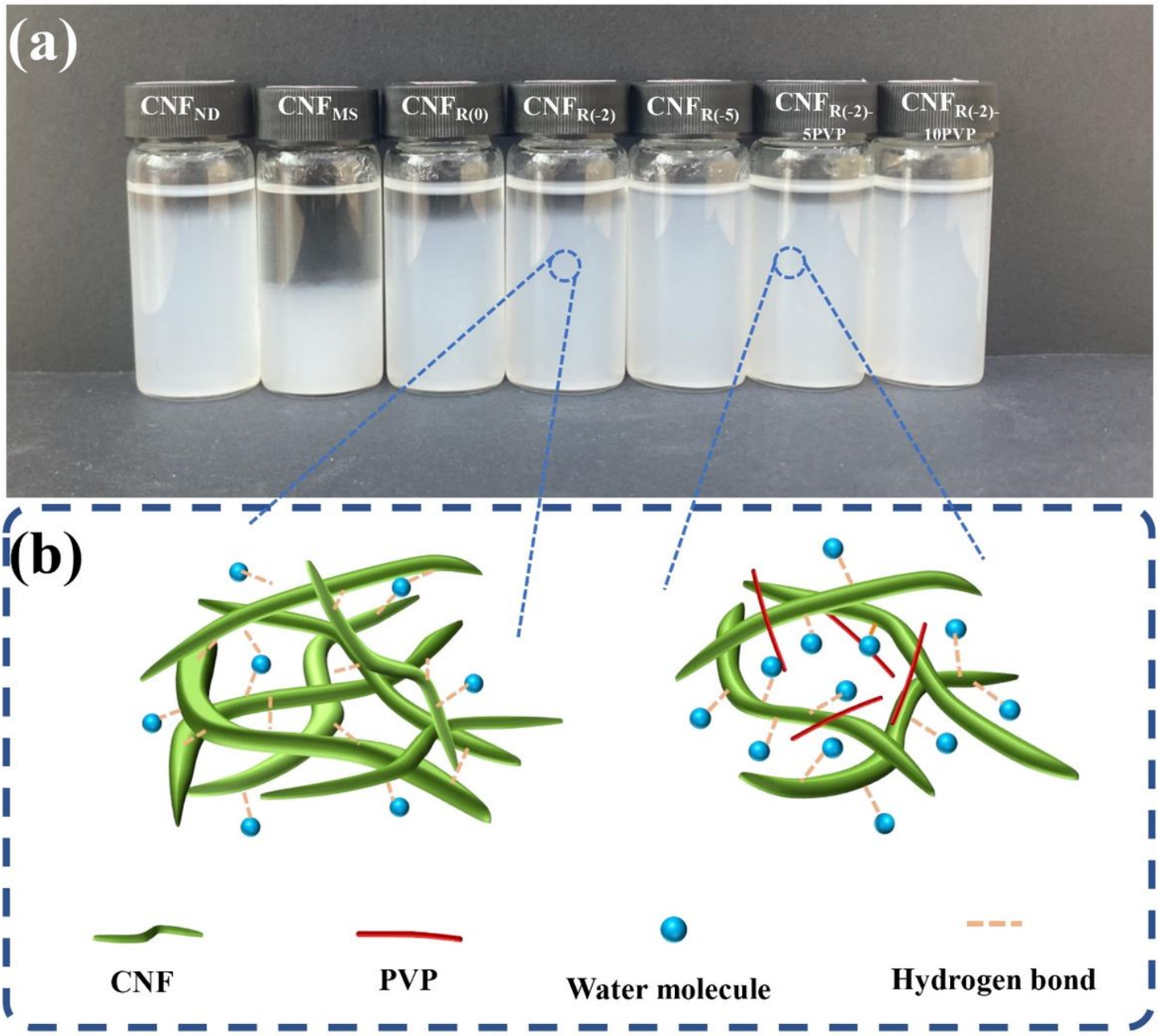

Figure 1

(a) Digital photograph of stability of initial and redispersed CNF suspensions at 0.2 wt% after 7 days. (b) Possible mechanism of the effect of PVP on the suspension stability.

Figure 2

Transmittance of 0.1 wt% CNF suspensions.

Figure 3

AFM images (up) and diameter distribution histograms (down) of (a) CNF_{ND}, (b) CNF_{MS}, (c) $CNF_{R(0)}$, (d) $CNF_{R(-2)}$, (e) $CNF_{R(-5)}$, (f)$CNF_{R(-2)-5PVP}$ and (g)$CNF_{R(-2)-10PVP}$. The agglomerations of PVP were marked by green arrows.

Figure 4

(a) FTIR spectra of neat PVP, CNF_{ND}, $CNF_{R(-2)}$, $CNF_{R(-2)-5PVP}$ and $CNF_{R(-2)-10PVP}$. (b) XRD patterns of CNF samples with different redispersing treatments.

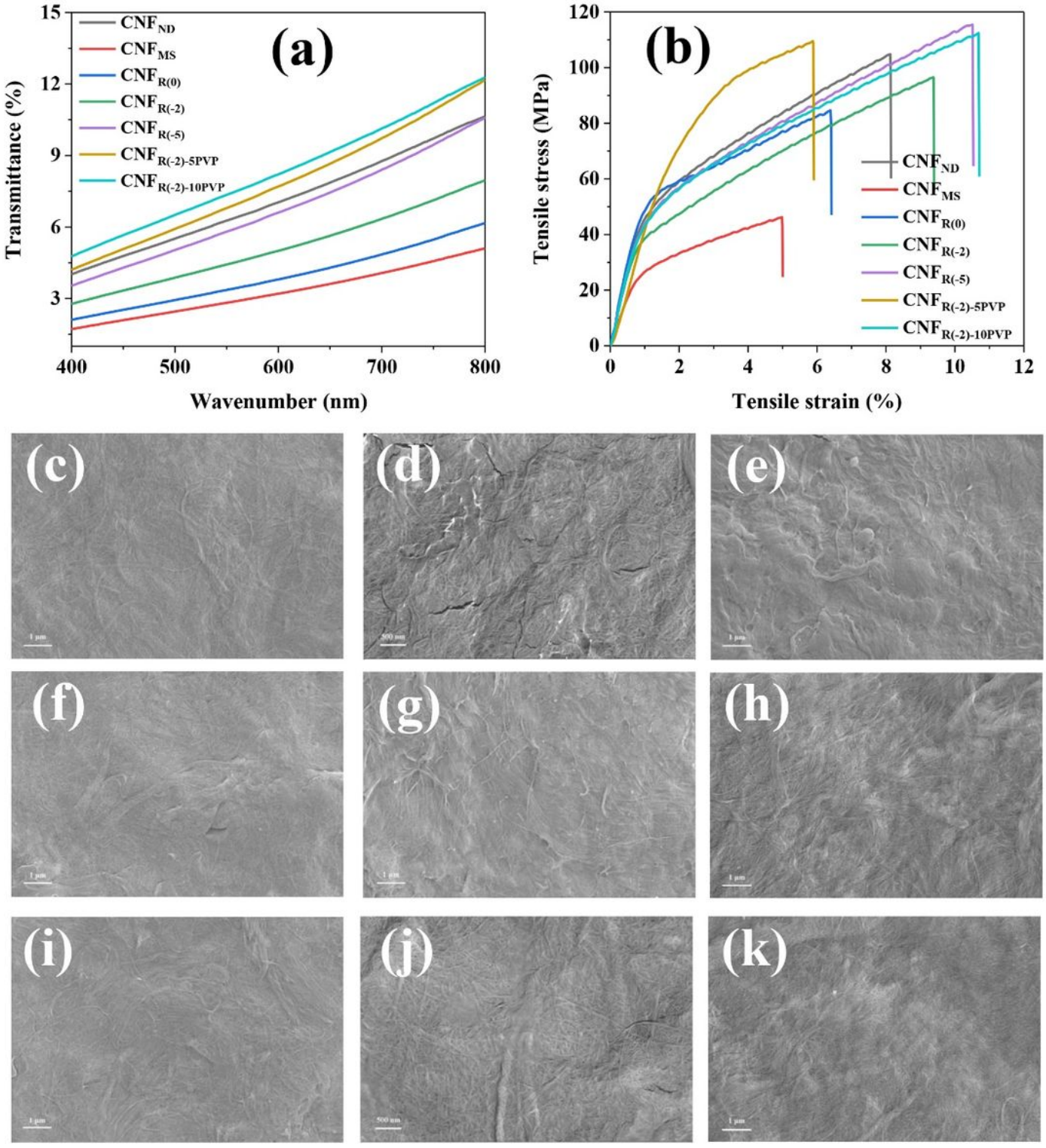

Figure 5

(a) Transmittance of CNF films. (b) Tensile stress-strain curves of CNF films. FE-SEM images on surface morphologies of (c) CNF_{ND} film (×10000), (d) CNF_{ND} film (×20000), (e) CNF_{MS} film(×10000), (f) $CNF_{R(0)}$ film (×10000), (g) $CNF_{R(-2)}$ film (×10000),(h) $CNF_{R(-5)}$ film(×10000), (i) $CNF_{R(-2)-5PVP}$ film(×10000), (j) $CNF_{R(-2)-5PVP}$ film (×20000), and (k) $CNF_{R(-2)-10PVP}$ film(×10000).

Figure 6

(a) Conductivity of CNF/PANI composite films. (b) Digital photo of CNF_{ND}/PANI composite film. FE-SEM images on surface morphologies of (c) CNF_{ND}/PANI, (d) $CNF_{R(-2)}$/PANI, (e) $CNF_{R(-2)\text{-}5PVP}$/PANI and (f) $CNF_{R(-2)\text{-}10PVP}$/PANI composite film. (g) Schematic illustration of CNF/PANI (up) and CNF/PANI/PVP (down). (h) Construction mechanism of CNF/PANI/PVP nanomaterial.

Figure 7

(a) CV curves of CNF_{ND}/PANI at different scan rates: 10, 20, 30, 50, 100, 200 mV/s. (b) Comparison of CV curves of each sample at 30 mV/s. (c) Specific capacitance of composite electrode calculated from CV curves within 10-200 mV/s. (d) GCD curves of CNF_{ND}/PANI at different current densities: 0.1, 0.2, 0.3, 0.5, 1.0, 2.0 A/g. (e) Comparison of GCD curves of each sample at 0.3 A/g. (f) Specific capacitance of composite electrode calculated from GCD curves within 0.1-2.0 A/g.